

OGMP: Oracle Guided Multimodal Policies for Agile and Versatile Robot Control

Lokesh Krishna Nikhil Sobanbabu Quan Nguyen

University of Southern California

Los Angeles, CA, USA

{lkrajan, quann}@usc.edu

Abstract: The efficacy of model-free learning for robot control relies on the tailored integration of task-specific priors and heuristics, hence calling for a unified approach. In this paper, we define a general class for priors called oracles and propose bounding the permissible state around the oracle’s ansatz, resulting in task-agnostic oracle-guided policy optimization. Additionally, to enhance modularity, we introduce the notion of task-vital modes. A policy mastering a compact set of modes and intermediate transitions can then solve perpetual tasks. The proposed approach is validated in challenging biped control tasks: parkour and diving on a 16-DoF dynamic bipedal robot, Hector. OGMP results in a single policy per task, solving indefinite parkour over diverse tracks and omnidirectional diving from varied heights, exhibiting versatile agility. Finally, we introduce a novel latent mode space reachability analysis to study our policy’s mode generalization by computing a feasible mode set function through which we certify a set of failure-free modes for our policy to perform at any given state.

1 Introduction

Deep reinforcement learning (RL) has shown remarkable success in synthesizing control policies for hybrid and underactuated legged robots [1], particularly in enabling inherently stable quadrupedal robots to achieve extreme parkour [2, 3, 4], agile [5], and robust [6] locomotion. Following a common philosophy: 1) define an exhaustive observation space, 2) engineer task-specific rewards and/or curriculum, 3) perform policy distillation, and 4) extensively randomize, these methods rely on task-specific tricks in each step, lacking a systematic approach for robot control. Specifically, since Deep RL methods are quasi-solvers for unconstrained optimization, they are prone to anomalous, case-specific local optima. Hence, practitioners often resort to task-specific reward shaping [2, 5, 6] and heuristics [3] to meet the intended performance. Furthermore, the established approach for robot control is privileged training and policy distillation: training teacher policies [3, 4] with privileged information, solving a pseudo-MDP with RL, and distilling it into a single policy for the true POMDP. In contrast, we aim to find an optimal policy by exploring in the true POMDP guided by priors with a task-agnostic objective.

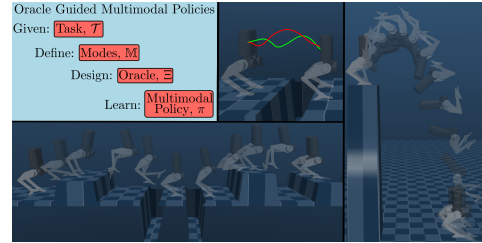


Figure 1: Conceptual overview of OGMP (top left), oracle guidance in green vs. actual motion in red (top center), a frontflip dive from a 2m high platform (right), and agile parkour on an arbitrary track with gaps and blocks (bottom left). Accompanying video results at : https://youtu.be/o_i03Z01LdE



Figure 2: Keyframes of an OGMP (π_{parkour}) pacing at a heading speed of 0.5 m/s on the real robot (left to right)

Alternatively, imitation learning (IL) proves to be a reliable task-agnostic strategy for robot manipulation with dynamically consistent demonstrations through proficient human teleportation which solve the intended task [7]. In contrast, we have dynamically inconsistent demonstrations for locomotion that partially solve a task, challenging the direct application of IL. For instance, to parkour with a bipedal robot, we may have demonstrations for runs, leaps, and jumps from motion capture on humans, which suffer from source-target mismatches due to morphological dissimilarity [8]. Moreover, naive imitation of partial demonstrations (run, leap, etc.) does not guarantee to solve the overarching task (parkour), requiring high-level RL-trained policy for transitions and emergent behaviors [9, 8, 10]. Besides demonstrations, robot tasks have rich priors like heuristics [11], task/motion planners [12], and model-based controllers [13], which can guide learning, leading to regularized behaviors [14]. While the idea of imitating such priors has been extensively studied, we instead propose building a “trust region” in the state space around the prior’s solution. Thus, the more we “trust” a prior, the tighter the trust region could be and vice versa. Formally defining a general class for priors: oracle, an oracle-guided policy optimization can be performed by bounding the policy’s permissible state space within the local neighborhood of an oracle’s ansatz. Empirically, we observe that the right choice of this bound helps escape erroneous local optima and provides an optimal balance between emergent and regularized behaviors ideal for robot control, thus making it an effective hyperparameter in practice.

On the other hand, solving complex tasks requires behavioural multimodality. Prior works in locomotion [10, 15] propose encoding a dataset of demonstrations to a latent space and latent conditioning to train multi-skilled policies. However, the notion of skill is poorly defined. For instance, solving a task requires not only mastering discrete modes (e.g., walking, jumping) but also continuous parameter variation of the same (e.g., speed, height) and inter-skill transitions. To this end, we first introduce task-vital multimodality as a way to decompose tasks into their principal modes and transcribe them into our proposed OGMP framework. Secondly, we leverage the latent conditioning space (or mode space) to analyze the generalization of OGMP over modes. Past works analyze their policies through qualitative results [5, 4] or report custom case-specific metrics [16, 8, 3, 17]. In contrast, we propose a modified reachability analysis on the low-dimensional latent mode space to compute the set of feasible behaviors our policy can perform in a given state. Analogous to value functions in RL, which gauge optimality from a state, we introduce the set-valued Feasible Mode-set function to assess feasibility. We characterize our policy’s generalization in and out of the training domain through the proposed Latent Mode Space Reachability Analysis. The interpretable mode sets combined with our generalization analysis aim to improve the modularity and reusability of black-box learned policies akin to hand-designed model-based control [13, 18]. Thus, the major contributions of our paper are twofold:

- **Oracle Guided Multimodal Policies:** A theoretical framework for task-centered control synthesis leveraging oracle-guided optimization for effective search through bounded exploration and task-vital multimodality for versatile control. Experimental validation on agile bipedal control tasks requiring versatility, such as parkour and diving. A single policy per task demonstrates the ability to perform diverse variants of the task-vital modes.
- **Latent Mode Space Reachability Analysis:** A modified reachability analysis to quantify our policy’s generalization through Feasible Mode-set Function computations

The remaining paper is structured as follows: Sec. 2 presents the theoretical development of our framework, Sec. 3 discusses applying the proposed framework to bipedal control tasks, followed by Sec. 4 presenting the experimental results, analysis and ablation studies.

2 Oracle Guided Multimodal Policies

This section presents our task-agnostic theoretical framework with two synergetic ideas: oracle-guided policy optimization and task-vital multimodality. Note that we develop this framework without specific considerations from our application tasks, ensuring its generality.

Oracle Guided Policy Optimization: Let \mathcal{T} be an infinite horizon task with a task parameter set, $\psi_{\mathcal{T}} \in \Psi_{\mathcal{T}}$. Sufficiently solving \mathcal{T} requires maximizing a task objective, $J_{\mathcal{T}}$ over the task parameter distribution, $p(\psi_{\mathcal{T}})$. Given the corresponding state space (or task space) of interest, $x \in \mathcal{X}$ let x_t , $x[a, b]$ denote a state at time t and a state trajectory from time $t \in [a, b]$ respectively. We define Ξ to be a receding horizon oracle that provides a finite horizon state trajectory ($x^{\Xi}[t, t + \Delta t]$) from any given state (x_t) until Δt into the future for any task-variant ($\psi_{\mathcal{T}}$), such that $x^{\Xi}[t, t + \Delta t]$ is always within an ϵ -neighborhood of an optimal state trajectory. Formally,

$$x^{\Xi}[t, t + \Delta t] = \Xi(x_t, \psi_{\mathcal{T}}) \quad (1a)$$

$$\text{s.t. } \exists x^{\Xi}[t, t + \Delta t] \quad \forall (x_t, \psi_{\mathcal{T}}) \quad (1b)$$

$$\|x_t^{\Xi} - x_t^*\|_W < \epsilon \quad \forall t \in [0, \infty) \quad (1c)$$

where ϵ is the maximum deviation bound, a constant for a given pair (\mathcal{T}, Ξ) , and W is a diagonal weight matrix¹. We aim to obtain the optimal policy π^* from a policy class Π guided by Ξ that sufficiently solves \mathcal{T} . Since Ξ provides a reference in the state space, we propose constraining the permissible states for π to be within a ρ -neighbourhood of the oracle’s guidance. Formally,

$$\pi^* := \arg \max_{\pi \in \Pi} J_{\mathcal{T}} \quad (2a)$$

$$\text{s.t. } \|x_t^{\pi} - x_t^{\Xi}\|_W < \rho \quad \forall t \in [0, \infty) \quad (2b)$$

Where x^{π} are the states visited while rolling out policy π , ρ is the permissible state-bound for oracle-guided exploration. Hence, one can now argue that

$$\begin{aligned} \|x_t^{\pi} - x_t^*\|_W &\leq \|x_t^{\pi} - x_t^{\Xi}\|_W + \|x_t^{\Xi} - x_t^*\|_W \\ &= \epsilon + \rho \quad \forall t \in [0, \infty) \end{aligned} \quad (3)$$

Thus, by bounded exploration within a ρ -neighborhood of x^{Ξ} , π^* can still be found within the constrained search space² i.e. $(\epsilon + \rho)$ -neighborhood of x^* as visualized in Fig. 3.b. ϵ being maximum deviation of x^{Ξ} , an oracle with low ϵ will generate references closer to x^* . In contrast, for a “poor” oracle with high ϵ , there should be sufficient search space for π to explore around x^{Ξ} and converge to x^* . Intuitively, as $\epsilon \rightarrow \infty$, the optimization is unguided, thus needing $\rho \rightarrow \infty$ (a standard RL setting). Conversely, as $\epsilon \rightarrow 0$, the search can be localized to a tight neighborhood of x^{Ξ} , implying $\rho \rightarrow 0$ ³. In practice, as ϵ is unknown, we perform a grid search over ρ for any given (\mathcal{T}, Ξ) .

Task Vital Multimodality: Any task, \mathcal{T} , can be seen as a “bundle” of spacetime trajectories in the task space, corresponding to $\psi_{\mathcal{T}} \in \Psi_{\mathcal{T}}$. Simple tasks allow straightforward oracle construction satisfying Eq 1. However, complex and infinite-horizon tasks make $\Psi_{\mathcal{T}}$ intractable. For instance, an oracle for indefinite parkour requires knowledge of an infinite track apriori, which is impractical. To address this, we define modes as finite spacetime segments that preserve several spatial and temporal invariances. Like in parkour, modes like jump and leap remain consistent regardless of location or time. Therefore, we define a finite set of modes, \mathbb{M} , vital for \mathcal{T} . Each $m \in \mathbb{M}$ (like jump) can have continuous parameters Ψ_m (like jump height). Then the mode parameter set $\Psi_{\mathbb{M}} := \bigcup_{i=1}^{|\mathbb{M}|} \Psi_{m_i}$ is related to the task parameter set as $\Psi_{\mathcal{T}} := \Psi_{\mathbb{M}}^N$, where N is the number of horizons. Thus, by mastering modes in \mathbb{M} (jump, leap, and pace) and transitions over varying $\Psi_{\mathbb{M}}$ (speeds, distances, and heights), task \mathcal{T} (indefinite parkour, $N \rightarrow \infty$) can be solved as visualized in Fig 3.a. For an elaborate conceptual illustration refer Appendix A.5.

3 Proposed Approach

This section first outlines our design methodology using OGMP for our control tasks of interest, as shown in Fig 3 followed by the proposed latent mode-space reachability analysis.

¹Note that $x^*[0, \infty]$, ϵ are unknown and are only provided for constructing the conceptual argument

² $\rho \geq \epsilon$ is assumed to be trivially satisfied

³we hypothesize that an optimal ρ for a given ϵ , $\rho^* = \alpha(\epsilon)$, where α should be non-decreasing function

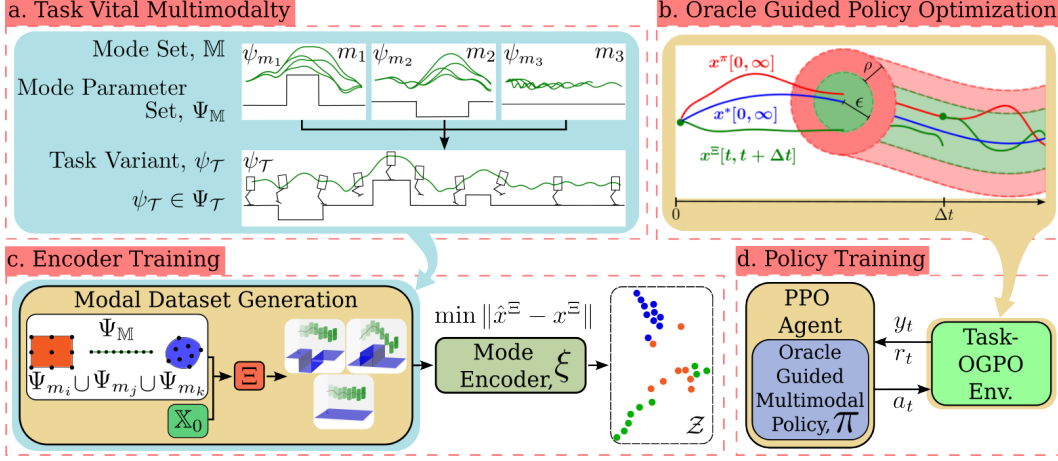


Figure 3: Overview of the design methodology: a) The breakdown of a task into its mode and mode parameter set b) Guided exploration by bounded permissible state space around the local neighborhood of the oracle’s reference c) Mode encoder: an LSTM autoencoder trained on a custom modal dataset by minimizing reconstruction loss d) Multimodal policy trained with oracle guided policy optimization on a task environment

3.1 Design Methodology

Task description: We apply the proposed framework to two bipedal control tasks: parkour and dive, with varying objectives and extent of multimodality as shown in table 1. Note that the choice of task-vital multimodality is user-defined, and table 1 simply reflects our choice for the same. Evident from table 1, $J_{\mathcal{T}}$ is task-dependent. Recent attempts in quadruped parkour [2, 3], and locomotion [6, 1] show some well-shaped candidates for $J_{\mathcal{T}}$, albeit case-specific. In general, a reasonable $J_{\mathcal{T}}$ could be hard to design (for instance, the dive task); a compelling unified alternative would be to “track” the oracle’s ϵ -neighbourhood reference to the optimal solution. Hence, we propose minimizing the task-independent surrogate objective: $\tilde{J}_{\mathcal{T}} := \sum_{t=0}^{\infty} \|x_t^{\pi} - x_t^{\Xi}\|$. $\tilde{J}_{\mathcal{T}}$ ’s applicability is studied in Sec. 4.3 and a reward is proposed in Appendix A.3 for an equivalent maximization objective.

$\mathcal{T} : J_{\mathcal{T}}$	$(m, \Psi_m) \in (\mathbb{M}, \Psi_{\mathbb{M}})$
dive: 360° flip and land	(settle, $\{\}$), (flip $\{(r, h)\}$)
parkour: traverse the track indefinitely	(pace, $\{v\}$), (jump $\{(w, h)\}$), (leap $\{(w, d)\}$)

Table 1: Task description and corresponding task vital multimodality. Parameters visualised in Fig. 4

Oracle Design: For any locomotion task, a simple heuristic for an oracle would be linearly interpolating the relevant state variables from the initial to the desired goal states. In parkour, to advance along the track, the heading position can be linearly interpolated along the track while adapting to the terrain height, as shown in Fig. 4 (left). For dive, the oracle can linearly interpolate the base height and corresponding rotational DoF from 0° to 360° . Naming this heuristic oracle as Ξ_{li} (Fig. 4), its high ϵ is obvious as the generated ansatz do not consider the system’s inertia and gravity. To this end, considering a simplified single rigid body model [13] with LTV dynamics, adding an auxiliary control can lead to an LTI system (Appendix A.2). Using Ξ_{li} as the reference for a quadratic tracking objective on the LTI system, optimizing with preview control [19] and LQR results in oracles, Ξ_{prev} and Ξ_{lqr} respectively, having a smaller ϵ , as they capture the dominant dynamics of the hybrid system as shown in Fig 4.

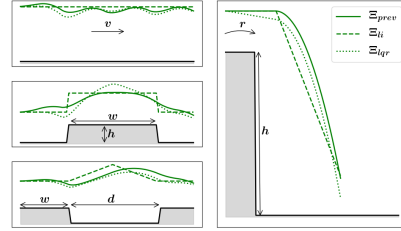


Figure 4: Base height reference trajectories from various oracles for different modes

Mode Encoder: We train a mode encoder, ξ , on diverse locomotion modes to obtain a compact conditioning space ideal for analyzing our policy. Similar to [15], the encoder, $z = \xi(x[t, t + \Delta t])$, maps the trajectory space to a latent space ($\dim(z) = 2$). Uniformly sampling from a mode parameter set, $\Psi_{\mathbb{M}}$ and a set of initial states, \mathbb{X}_0 , we generate a rich and balanced modal dataset by

querying the oracle, Ξ as shown in Fig. 3.c. Minimizing the reconstruction loss for a 32 neurons single hidden layer LSTM auto-encoder on the custom dataset generates a set of latent mode points with a structured clustering as visualized in Fig. 3.c.

Mode Conditioned Policy: Our choice of action space for a stationary policy is from [15]. Given the inherent partial observability of the system, for the observation space $o_t \in \mathcal{O}$ we choose $o_t = [\tilde{x}_t, z_t, c_t, h_t]$, where \tilde{x}_t is the robot’s proprioceptive feedback, z_t is the latent mode command, c_t is a clock signal [15] and h_t is optional task-based feedback (like terrain scan for parkour). The proposed permissible state constraint (Sec. 2) is programmed as a termination condition, terminate episode := $\mathbb{1}(\|x_t^\pi - x_t^\Xi\|_W > \rho)$. W_{11} and W_{33} are set to 1 for the parkour and dive tasks, respectively, with the remaining entries as zero. For solving the resulting random horizon POMDP, we use off-the-shelf PPO to train a policy: 128 nodes per layer, 2 layer LSTM network, where each episode is an arbitrary variant of the task $\psi_{\mathcal{T}}$ uniformly sampled from $\Psi_{\mathcal{T}}$.

3.2 Latent Mode Space Reachability Analysis

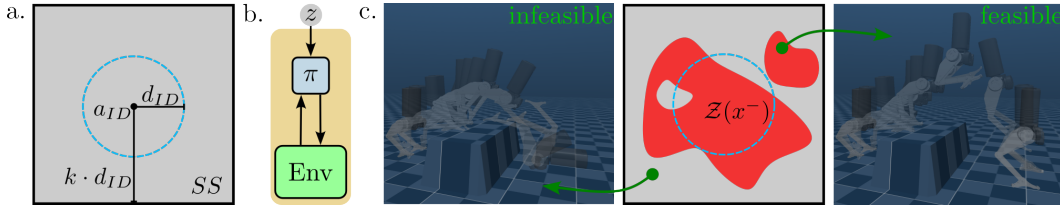


Figure 5: Overview of LMSR Analysis: a) search space, SS defined based on π ’s estimated a_{ID} and d_{ID} . b) closed-loop system (F_π) under analysis. c) the computed feasible mode-set function, $Z(x^-)$ (red) from the state, x^- with a feasible ($z \in Z(x^-)$) and infeasible ($z \notin Z(x^-)$) mode visualized

Leveraging the latent mode space, we perform a modified reachable set computation to find the failure-free modes (feasible) from a given state and thereby study our policy’s generalization. We first define $\mathcal{X}_{\text{fail}}$, a set of failure states we want the system to avoid. Considering the closed-loop system with the multimodal policy and the environment, the latent mode command (z) is the only input as in Fig 5.b. Since mode switches occur once every Δt , the discrete-time closed-loop mode-controlled dynamics for a task variant $\psi_{\mathcal{T}}$ can be written out as: $x^+ = F_\pi(x^-, z, \psi_{\mathcal{T}})$, where x^+ is the state of the system after Δt seconds having commanded the mode z from the state x^- . For a given x^- , finding a set of modes for which the system won’t reach $\mathcal{X}_{\text{fail}}$ within Δt is of interest to us. Formally, we define the feasible mode-set function, which maps a state to the set of all feasible modes in the latent mode space as follows,

$$\mathcal{Z}(x) := \{z | x^+ \notin \mathcal{X}_{\text{fail}}, x = x^-\} \quad (4)$$

Since F_π is not assumed to be known analytically, we compute $\mathcal{Z}(x)$ by explicitly rolling out the policy, which we call the Latent Mode Space Reachability (LMSR) test as shown in Fig 5.

To compute $\mathcal{Z}(x)$, we first define a search space, $SS := \{z | \|z - a_{ID}\|_\infty < k \cdot d_{ID}\}$, where a_{ID} and d_{ID} are the center and radius of the circumcircle of the latent points in-domain (ID) of the training as shown in Fig 5.a. Intuitively, one can expect a policy to be successful when commanded from $ID := \{z | \|z - a_{ID}\| < d_{ID}\}$ as it is within the training domain. ID , however, is a conservative estimate of the modes that the policy might have learned; hence, to account the out-of-domain(OD) mode generalization of π , we include points $OD := \{z | \|z - a_{ID}\| \geq d_{ID}, z \in SS\}$ by choosing $k > 1$. Thus, an exhaustive $\mathcal{Z}(x)$ is computed from a given x and $\psi_{\mathcal{T}}$ within SS by rolling out F_π in simulation as visualized in Fig 5.c on a discretized SS . Once $\mathcal{Z}(x)$ is computed, a direct measure of the diversity would be $|\mathcal{Z}(x)|$, as it is the number of feasible modes that π could execute from x . To quantify the generalization of π in a domain \mathcal{D} we define $\nu_{\mathcal{D}}(\mathcal{Z}(x)) := \frac{\text{no. of points in } (\mathcal{Z}(x) \cap \mathcal{D})}{\text{no. of points in } (\mathcal{D})}$, where $\nu_{\mathcal{D}} \in [0, 1]$ measures the probability of success when a point z is chosen from a domain \mathcal{D} at a given $(x, \psi_{\mathcal{T}})$. Taking $\mathcal{D} = ID, OD$ we measure the in-domain and out-of-domain generalization of our policies in Sec. 4.2

4 Results

4.1 Performance

To achieve extreme agility and mode versatility, a single multimodal policy is trained per task: π_{parkour} for parkour and π_{diver} for diving. The supplementary video and Fig 1 show π_{parkour} successfully navigating challenging parkour tracks with blocks and gaps placed randomly, demonstrating versatile agility over leap lengths and jump heights (Appendix A.1). π_{diver} performs omnidirectional flips from different heights and transitions smoothly to landing. Despite lacking a reference for the actuated DoFs, π_{diver} learns an emergent behavior to curl and extend its legs for flips and landings, modulating the torso angular velocity and landing impact. As seen in the video, π_{parkour} significantly deviates from the oracle’s reference to find the optimal behavior, yet results in regularized motion due to the oracle bound. On average, we find π_{parkour} to reach accelerations of $4.7g$ with heading speeds of 1.77 m/s , and Froude numbers between $0.48 - 0.72$ while completing 84% of the track as shown in table 2. π_{parkour} dynamically advances along the track, avoiding conservative motions with precise foot placements for landing and take-off, leading to agile manoeuvres. The measured Froude numbers and resulting motion are consistent with [20], where a switch from energy-efficient walking to agile jumping gaits was observed in bipedalism for a value around 0.5. Preliminary sim-to-real transfer of π_{parkour} can be seen in Fig 2 and supplementary video.

4.2 Latent Mode Space Reachability (LMSR) Tests

Taking, $\mathcal{X}_{\text{fail}} := \{x \mid \text{base height} < \text{nominal min. base height}\}$, two variants of the LMSR test (Sec 3.2) are performed on π_{parkour} : 1) Flat Ground Test: to quantify the mode-diversity from a nominal state and terrain and 2) Transition Test: to quantify the “volume” of modes available to transition from a given state. a_{ID} and d_{ID} in table 2 are estimated from latent modes (blue dots in Fig. 6.a) in-domain of $p(\psi_{\mathcal{T}})$, to compute the corresponding search space.

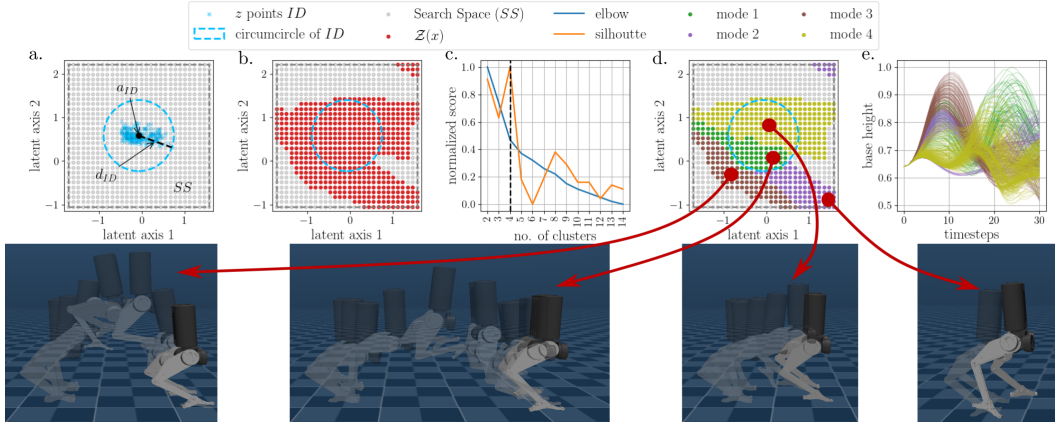


Figure 6: Overview of the Flat ground LMSR Test: a) The defined search space SS based on a_{ID} , and d_{ID} of π_{parkour} . b) The Finite Mode Set Function ($\mathcal{Z}(x)$) computed from the nominal initial state and terrain. c) The elbow and silhouette scores for varied ‘K’ of K-Means clustering over the corresponding state trajectories. d) Mode clusters corresponding to the optimal number of clusters, $K=4$ c) the base height trajectory corresponding to the different points in $\mathcal{Z}(x)$, colored consistent with their mode cluster.

Flat Ground LMSR Test: Using $\psi_{\mathcal{T}} = \text{flat ground}$ and $x = \text{nominal initial state}$, we rollout $F_{\pi_{\text{parkour}}}$ for one horizon (Δt) for each z in the search space with $k = 2$ (Fig. 6.a). The computed $\mathcal{Z}(x)$ in Fig.6.b shows π_{parkour} generalizes with success probabilities, in ID as $\nu_{ID} = 0.99$ and OD as $\nu_{OD} = 0.49$. K-means clustering on state trajectories corresponding to $\mathcal{Z}(x)$ (Fig. 6.e) suggests the optimal number of clusters is $K = 4$ with the highest silhouette score, consistent with the elbow plot (Fig. 6.c). This supports our hypothesis of needing a finite number of modes to solve tasks. The modes (Fig. 6 bottom, d) are jump, leap, hop, and step where π_{parkour} varies the mode parameters

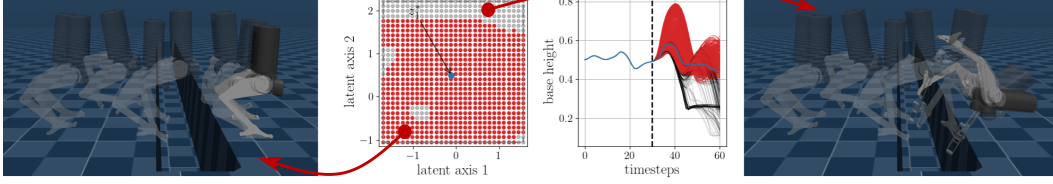


Figure 7: Overview of the Transition LMSR Test: left) a feasible transition corresponding to a point in $\mathcal{Z}(x)$. center) the feasible mode set function at the transition state and the corresponding base height trajectories are shown in red. right) an infeasible transition from a point not in $\mathcal{Z}(x)$. The optimal mode-to-transition picked by the corresponding Ξ and its trajectory is shown in blue.

to perform a range of behaviors and transitions. Notably, a single mode: pace is split into 1) hop to traverse flat terrain and 2) step to adjust before leaps and jumps, as seen in the supplementary video.

Transition LMSR Test: For an arbitrary track $\psi_{\mathcal{T}}$ and an episode length of $2\Delta t$, we perform the second LMSR test variant. Starting from the nominal state at $t = 0$, π_{parkour} follows the optimal mode command z_0^* (from the oracle) until $t = \Delta t$. At the transition state $x_{\Delta t}$, we compute $\mathcal{Z}(x = x_{\Delta t})$ to find feasible transition modes. The computed $\mathcal{Z}(x)$ and corresponding state trajectories (Fig. 7 center) show ID and OD transitions, with success probabilities $\nu_{ID} = 1.0$ and $\nu_{OD} = 0.77$. Though the oracle-commanded transition z_1^* (blue in Fig. 7) is ID, π_{parkour} learns other feasible transitions (red in Fig. 7). Thus, π_{parkour} isn't limited by Ξ and learns novel maneuvers through exploration within the $\epsilon + \rho$ neighborhood around Ξ 's reference. Given such "bandwidth" of mode transitions, these OGMPs can solve unseen tasks by designing a new oracle, Ξ_{new} . We conjecture that if Ξ_{new} selects mode commands $z \in \mathcal{Z}(x)$, $\forall x$ at mode-switches, the same low-level policy can solve novel tasks with common modes without retraining.

4.3 Ablations and Analysis

Finally, we analyze our choice of surrogate $\tilde{J}_{\mathcal{T}}$ and design choices that impact performance (measured via undiscounted returns). For parkour, a potential true objective, $J_{\mathcal{T}}$, is the displacement along the track. Thus the validity of using $\tilde{J}_{\mathcal{T}}$ can be quantified through its disparity with $J_{\mathcal{T}}$.

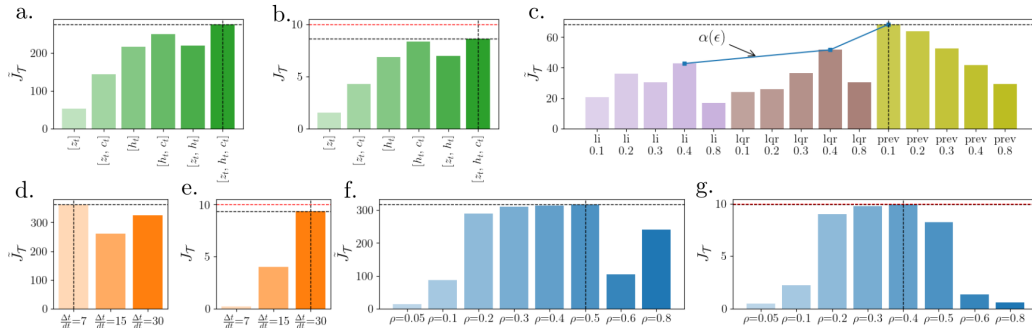


Figure 8: The estimated surrogate ($\tilde{J}_{\mathcal{T}}$) and true ($J_{\mathcal{T}}$) objectives vs. choice of 1) observation space, o_t (a and b), 2) oracles, Ξ (c), 3) horizon length, Δt (d and e) and 4) permissible state bound, ρ (f and g). In b, e, and g the upper bound of $J_{\mathcal{T}}$ is marked in red.

Choice of observation space (o_t): Ablation of observation space components (excluding \tilde{x}_t) shows that variants with c_t consistently outperform their counterparts (Fig. 8.a). Variants without h_t are myopic and aggressive, with higher accelerations (table 2) as they purely rely on compressed z_t for terrain feedback, making them sub-optimal compared to terrain-aware variants. From Fig. 8.a, we observe that latent conditioning does not improve performance (see $[h_t, c_t]$ and $[z_t, h_t, c_t]$), hence is purely for analysis and reusability. However, a conditioned π_{parkour} can use the oracle as a closed-loop reactive planner during inference, driving the system to the commanded mode. From Fig. 8.a and b, a similar trend of $J_{\mathcal{T}}$ and $\tilde{J}_{\mathcal{T}}$ shows no disparity caused by observation space variations.

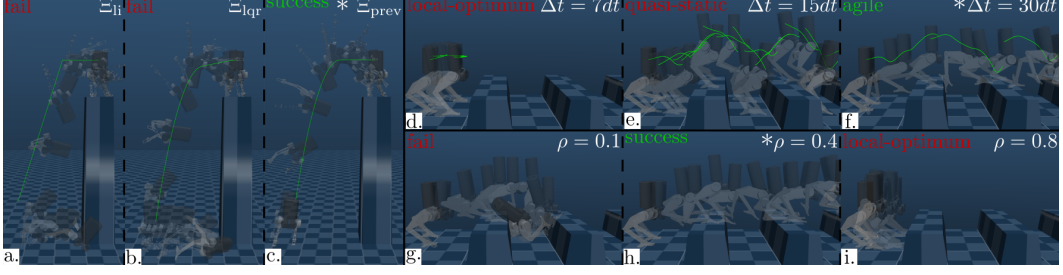


Figure 9: Motion traces comparing the choice of 1) oracles (a, b, c) where Ξ_{li} , Ξ_{lqr} fail while only Ξ_{prev} successful in a side flip dive from a 2m block 2) horizon length (d, e, f) where the longest horizon ($\Delta t = 30dt$) results in the desired agile performance 3) permissible state bound (g, h, i) where the tighter ($\rho = 0.1$) and lenient ($\rho = 0.8$) bounds fail

Choice of oracle (Ξ): The three oracles, Ξ_{li} , Ξ_{lqr} , and Ξ_{prev} , have a non-increasing trend in maximum deviation bound, ϵ . As the optimal exploration bound (ρ^*) depends on ϵ , we vary ρ from 0.1 to 0.8 for each oracle. For parkour, different oracles show no significant performance difference (see video results). However, for dive, Ξ_{prev} variants perform significantly better (Fig. 8.c and 9.c). A tighter bound ($\rho = 0.1$) works best for Ξ_{prev} , as it has the lowest ϵ . Conversely, higher exploratory deviation ($\rho = 0.4$) performs best for Ξ_{lqr} and Ξ_{li} . Thus, $\epsilon_{li} \geq \epsilon_{lqr} \geq \epsilon_{prev} \implies \rho_{li}^* \geq \rho_{lqr}^* > \rho_{prev}^*$, affirming $\rho^* = \alpha(\epsilon)$, a non-decreasing function (Fig. 8.c).

Choice of oracle's horizon (Δt): We evaluate policy performance across different horizons: $\Delta t = 7dt$, $15dt$, and $30dt$ for parkour. The shortest horizon, $\Delta t = 7dt$, leads to a myopic behavior, maintaining a high $\tilde{J}_{\mathcal{T}}$ but low $J_{\mathcal{T}}$ as it remains stationary by exploiting the high replanning frequency (Fig. 9.d and 8.d, e) as also observed by [14]. Although advancing forward, $\Delta t = 15dt$ fails to anticipate farther terrain, resulting in quasi-static maneuvers (Fig. 9.e). Conversely, $\Delta t = 30dt$ enables the robot to leap efficiently from block to block, demonstrating agility and achieving the optimal outcome (Fig. 9.f). Increasing Δt aligns $\tilde{J}_{\mathcal{T}}$ with the true task objective, $J_{\mathcal{T}}$ (Fig. 8.d, e).

Choice of permissible state bound (ρ): For Ξ_{prev} in parkour, we varied ρ from 0.05 to 0.8 (Fig. 8.f and g). We found an optimal $\rho^* = 0.5$ with performance decreasing away from this value. For $\rho < \rho^*$, the optimal solution may lie outside the ρ -neighborhood of x^Ξ (Fig. 9.g and Fig. 10). Conversely, $\rho > \rho^*$ increases local optima within $\epsilon + \rho$, leading to sub-optimal solutions (high $\tilde{J}_{\mathcal{T}}$), seen in Fig. 9.i for $\rho = 0.8$, where the policy stagnates without advancing (low $J_{\mathcal{T}}$). Training curves in Fig. 10 show that $0.1 \leq \rho \leq 0.6$ converges to the global optima, while the rest settle at local optima. Note that $\rho \rightarrow \infty$ is standard PPO as it optimizes $\tilde{J}_{\mathcal{T}}$ unguided by Ξ . Vanilla unguided PPO ($\rho = 10^{10}$) falls into the same local optima as $\rho = 0.8$. Thus, oracle-guided optimization improves standard PPO by escaping local optima with the right choice of ρ .

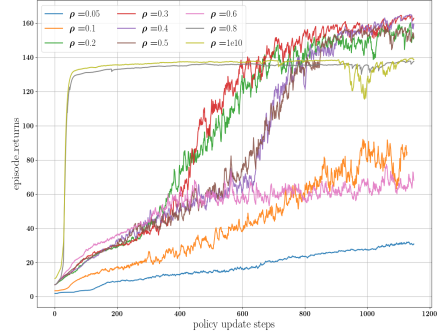


Figure 10: Training curves for different ρ 's with a fixed set of PPO's hyperparameters.

5 Conclusion

This paper introduces a framework for guided policy optimization through prior-bounded permissible states and task-vital multimodality to tackle complex tasks. A single OGMP (per task) successfully solved agile bipedal parkour and diving, showcasing versatile agility. Additionally, a novel reachability analysis was introduced to characterize the policy generalization and, thereby, enhance its reusability. Future work will aim extending to contact-rich open-world loco-manipulation tasks.

Limitations: Restricting the reachable states to a subset of the state space, we forgo the possibility of OGMP being a global policy. Consequently, any state outside the ρ -neighbourhood of the oracle's references may result in failure. Since current Deep RL methods lack any global convergence guarantees, this is nonrestrictive but highlights the need for future extensions for stronger algorithms.

References

- [1] J. Siekmann, K. Green, J. Warila, A. Fern, and J. Hurst. Blind Bipedal Stair Traversal via Sim-to-Real Reinforcement Learning. In *RSS*, 2021.
- [2] D. Hoeller, N. Rudin, D. Sako, and M. Hutter. Anymal parkour: Learning agile navigation for quadrupedal robots. *Science Robotics*, 2024.
- [3] X. Cheng, K. Shi, A. Agarwal, and D. Pathak. Extreme parkour with legged robots. In *Robotics: Workshop @CoRL 2023*, 2023.
- [4] Z. Zhuang, Z. Fu, J. Wang, C. G. Atkeson, S. Schwertfeger, C. Finn, and H. Zhao. Robot parkour learning. In *CoRL*, 2023.
- [5] N. Rudin, D. Hoeller, M. Bjelonic, and M. Hutter. Advanced skills by learning locomotion and local navigation end-to-end. In *IEEE IROS*, 2022.
- [6] T. Miki, J. Lee, J. Hwangbo, L. Wellhausen, V. Koltun, and M. Hutter. Learning robust perceptive locomotion for quadrupedal robots in the wild. *Science Robotics*, 2022.
- [7] C. Chi, S. Feng, Y. Du, Z. Xu, E. Cousineau, B. Burchfiel, and S. Song. Diffusion policy: Visuomotor policy learning via action diffusion, 2023.
- [8] S. Bohez, S. Tunyasuvunakool, P. Brakel, F. Sadeghi, L. Hasenclever, Y. Tassa, E. Parisotto, J. Humprik, T. Haarnoja, R. Hafner, et al. Imitate and repurpose: Learning reusable robot movement skills from human and animal behaviors. *arXiv preprint arXiv:2203.1713*, 2022.
- [9] T. Haarnoja, B. Moran, G. Lever, S. H. Huang, D. Tirumala, J. Humprik, M. Wulfmeier, S. Tunyasuvunakool, N. Y. Siegel, R. Hafner, M. Bloesch, K. Hartikainen, A. Byravan, L. Hasenclever, Y. Tassa, F. Sadeghi, N. Batchelor, F. Casarini, S. Saliceti, C. Game, N. Sreendra, K. Patel, M. Gwira, A. Huber, N. Hurley, F. Nori, R. Hadsell, and N. Heess. Learning agile soccer skills for a bipedal robot with deep reinforcement learning. *Science Robotics*, 9(89): eadi8022, 2024.
- [10] L. Hasenclever, F. Pardo, R. Hadsell, N. Heess, and J. Merel. CoMic: Complementary task learning & mimicry for reusable skills. In *ICML*, PMLR, 2020.
- [11] M. H. Raibert. Legged robots. *Communications of the ACM*, 29(6):499–514, 1986.
- [12] J. Norby and A. M. Johnson. Fast global motion planning for dynamic legged robots. In *2020 IEEE/RSJ International Conference on Intelligent Robots and Systems (IROS)*, 2020.
- [13] J. Li and Q. Nguyen. Force-and-moment-based model predictive control for achieving highly dynamic locomotion on bipedal robots. In *IEEE CDC*, 2021.
- [14] F. Jenelten, J. He, F. Farshidian, and M. Hutter. Dtc: Deep tracking control. *Science Robotics*, 2024.
- [15] L. Krishna and Q. Nguyen. Learning multimodal bipedal locomotion and implicit transitions: A versatile policy approach. In *IEEE IROS*, 2023.
- [16] G. Margolis, G. Yang, K. Paigwar, T. Chen, and P. Agrawal. Rapid Locomotion via Reinforcement Learning. In *Proceedings of RSS*, 2022.
- [17] A. Sharma, S. Gu, S. Levine, V. Kumar, and K. Hausman. Dynamics-aware unsupervised discovery of skills. In *ICLR*, 2020.
- [18] M. Chignoli, D. Kim, E. Stanger-Jones, and S. Kim. The mit humanoid robot: Design, motion planning, and control for acrobatic behaviors. In *2020 IEEE-RAS 20th International Conference on Humanoid Robots (Humanoids)*, 2021.

- [19] M. Murooka, M. Morisawa, and F. Kanehiro. Centroidal trajectory generation and stabilization based on preview control for humanoid multi-contact motion. *IEEE RAL*, 2022.
- [20] R. M. Alexander. The gaits of bipedal and quadrupedal animals. *IJRR*, 1984.
- [21] C. Li, M. Vlastelica, S. Blaes, J. Frey, F. Grimmering, and G. Martius. Learning agile skills via adversarial imitation of rough partial demonstrations. In *CoRL 2023*. PMLR.
- [22] E. Vollenweider, M. Bjelonic, V. Klemm, N. Rudin, J. Lee, and M. Hutter. Advanced skills through multiple adversarial motion priors in reinforcement learning. In *ICRA 2023*, pages 5120–5126.
- [23] S. Park, K. Lee, Y. Lee, and P. Abbeel. Controllability-aware unsupervised skill discovery, 2023.
- [24] A. Sharma, S. Gu, S. Levine, V. Kumar, and K. Hausman. Dynamics-aware unsupervised discovery of skills. In *ICLR 2019*.

A Appendix:

A.1 Mode Parameter Set Test

Since the defined $\Psi_{\mathbb{M}}$ of our training is a compact set, we leverage it to visualize the generalization of π_{parkour} over mode parameters. Dilating $\Psi_{\mathbb{M}}$ and defining higher test ranges for each parameter, we test for both in-domain (ID) and out-of-domain (OD) generalization. Discretizing this test set, we evaluate π_{parkour} and plot the undiscounted returns obtained for blocks and gaps with varying dimensions in Fig 11. Different blocks and gaps require jumps and leaps of varying magnitudes, showcasing our policies’ versatility. The training sets Ψ_{jump} and Ψ_{leap} are the regions within the boundary marked in black in each plot. Thus, π_{parkour} shows consistent performance for variants within the black boundary (ID) while also extrapolating its skills by jumping and leaping over unseen terrain variants outside the black boundary (OD) as seen in the supplementary video and Fig 11.

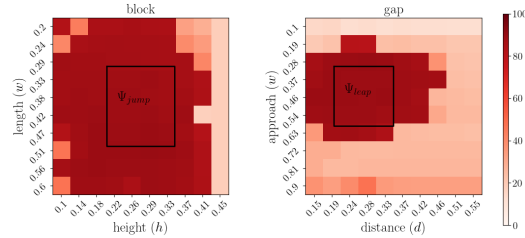


Figure 11: Heatmap of π_{parkour} ’s undiscounted returns performing jumps and leaps of varying magnitudes both in and out of $\Psi_{\mathbb{M}}$ while traversing blocks and gaps of different dimensions

A.2 Details of Model-based Oracles

The Ξ_{prev} and Ξ_{lqr} oracles require a model of the system to output the state trajectories. To this end, we have used a modified version of the simplified Single Rigid Body (SRB) model[13].

SRB model: The dynamics of the model in the world coordinates are given by:

$$m(\ddot{p} + g) = \sum_{i=1}^2 f_i, \frac{d}{dt}(I\omega) \approx I\dot{\omega} = \sum_{i=1}^2 (r_i \times f_i + \tau_i) = \sum_1^2 \bar{\tau}_i \quad (5)$$

$$x_{t+1} = Ax_t + Bu_t, y_{t+1} = Cx_t, u_t = [f_1, f_2, \bar{\tau}_1, \bar{\tau}_2]^T \quad (6)$$

where \ddot{p}, ω is the robot COM acceleration and the angular velocity, r_i, f_i, τ_i are the position, force and moment vectors from the i^{th} contact point and m, I, g are the mass, moment of inertia and gravity. Typically, r_i is from a predefined contact schedule, leading to time-varying dynamics. Since, by definition, an oracle need not provide realistic control, we define an auxiliary control $\bar{\tau}_i$,

encompassing the overall moment, making the dynamics time-invariant. Additionally, the rotation and rotation rate matrices are made constant by considering the average reference orientation over a horizon. Upon these approximations to Eq. 5 and discretization leads to a linear time-invariant (LTI) system over the current horizon, where $x_t \in \mathbb{R}^{13}$, $y_t, u_t \in \mathbb{R}^{12}$ are the gravity-augmented state, relevant output, and control vectors. Thus, oracles can be constructed considering two distinct phases: flight and contact. In flight, $u_t = 0$ as there are no contacts, and during contact, an optimizer of choice can be used to compute the optimal control for a given objective, $u_t = u_t^*$. The reference state trajectory is obtained by applying the corresponding control and forward simulating Eq. 6.

Choice of Optimizer: Given an LTI model and the absence of constraints, we use the analytic solution of preview control[19] as opposed to sophisticated numerical optimizers, thereby allowing long-horizon computations. As a desirable attribute for an oracle, preview control incorporates look-ahead behavior with a previewable demand term in its control law as opposed to LQR. Thus, using Ξ_{li} as the previewable demand Ξ_{prev} produces successful results in complex tasks such as dive which is seen in Fig 9.

A.3 Task-agnostic objective

Our choice of the per-step reward for a task-agnostic tracking objective consists of an oracle-tracking term r_{track} and a regulation term $r_{regulation}$. r_{track} aims to minimize an error in the task space, and $r_{regulation}$ is added to enforce regularised behaviours for sim-to-real considerations.

$$\begin{aligned} r_t &:= r_{track} + r_{regulation} \\ r_{regulation} &:= 0.05e^{-0.01\|u_t\|} - 0.3 \cdot \mathbb{1}(\text{if non-toe contact}) \\ r_{track} &:= 0.475e^{-5\|er_p\|} + 0.475e^{-5\|er_o\|} \end{aligned} \quad (7)$$

where er_p, er_o are the errors in base position and orientations. Note for the diverse modes across both the tasks (parkour and dive) the reward weights remain the same, hinting a sense of algorithmic robustness that arises from guided learning.

A.4 Estimated Metrics

metric, units	z_t	z_t, c_t	h_t	h_t, c_t	h_t, z_t	h_t, z_t, c_t
M.T.A, m/s^2	4.7g	3.5g	3.2g	3.6g	3.5g	3.1g
M.H.S (v), m/s	1.4	1.57	1.66	1.74	1.74	1.77
M.F ($\frac{v^2}{g \cdot l}$), —	0.48	0.56	0.64	0.69	0.70	0.72
% E.L, —	0.18	0.43	0.63	0.80	0.66	0.84
a_{ID} , —	(0.09, 0.60)	(-0.07, 0.58)	-	-	(-0.03, 0.64)	(-0.23, 0.50)
d_{ID} , —	0.63	0.82	-	-	0.84	1.01

Table 2: Estimated metrics for variants of $\pi_{parkour}$ with different observation spaces

For quantitative benchmarking, we report the expectation of different performance metrics, Maximum of Heading Acceleration (M.H.A), Froude number (M.F), Maximum Heading Speed (M.H.S), Episode Length(E.L), approximated by the sample mean measured over n episode rollouts. For the proposed LMSR analysis, we also estimate indomain radius (a_{ID}) and outdomain radius (d_{ID}) over the task parameter distribution $p(\Psi_{\mathcal{T}})$. If l is a defined metric, the values in table 2 and Fig. 8 are computed as $\mathbb{E}_{p(\Psi_{\mathcal{T}})}[l] \approx \frac{1}{n} \sum_i^n l_i$, where l_i is the i^{th} sample. Empirically, we found $n = 100$ for every metric’s mean to settle as a reliable estimate. We define a test environment with a track length of 10m, an episode length of 400 steps for the parkour, and an episode length of 150 for the dive. In each case, the episode is terminated only if the episode length is reached or the robot falls down (if the terrain-relative base height < 0.3 m).

A.5 Illustrating Task-Vital Multimodality

Prior works on multitasked policies typically involve training a low-level policy to either imitate a dataset of reference motions [9, 8, 21, 22, 10] or to discover skills from scratch [23, 24].

However, these methods rely on a high-level policy [9, 8] or planner [24] to solve tasks, which necessitates defining task-specific reward terms [22]. Consequently, the concept of skills is loosely defined, creating ambiguity regarding the required number and versatility of skills for solving a task. In response, our proposed task-vital multi-modality in Sec 2, defines a set of skills (or modes) that are vital to solve a task. A mode is conceptualized as a “finite” segment that preserves spatiotemporal invariances, ensuring compactness for effective learning while maintaining scalability for complex and indefinite tasks. Thus, by learning these modes and their intermediate transitions (extending [15]), we aim to solve the task sufficiently.

To illustrate this, consider a toy task visualized as a “bundle” of trajectories in Fig 12. In theory, each variant of the task ($\psi_{\mathcal{T}}^i$) can be infinitely long with an infinite of them, leading to an intractable $\Psi_{\mathcal{T}}$. Naively training a policy requires learning each of these trajectories. However, one can notice that each trajectory is a sequence of primitive segments labeled as m_1 , m_2 and m_3 with slopes -45° , 0° and 45° respectively. Notably, these segments preserve temporal and spatial invariances: starting from the same point x , segments at different times t_a and t_b yield identical “displacement” Δ_s , making m_1 temporally invariant. Similarly, m_3 segments starting at time t from different points x_a and x_b show spatial invariance by traversing Δ_s . Thus, with TVM we aim to define such invariant modes as compact building blocks sequencing which can result in a multitude of $\psi_{\mathcal{T}}^i$ thus solving \mathcal{T} sufficiently. This can be clearly seen in Fig 3.a, where for the parkour task, learning the variations of three modes (pace, jump and leap) and transitions enabled the bipedal robot to traverse the track indefinitely. From our analysis in Sec 4.2, we speculate that the our oracled-guided training preserves such TVM-induced invariances in the policy resulting in the effective in and out-of domain generalisation, prompting further study in future works.

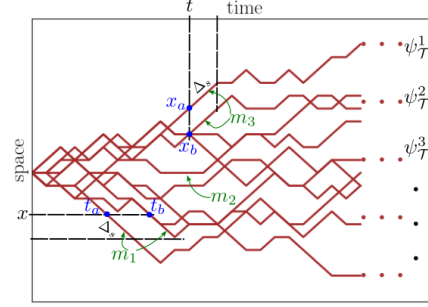


Figure 12: Conceptual visualization of Task-Vital Multimodality